remote sensing

MDPI

Article

Evaluation of GOCI Remote Sensing Reflectance Spectral Quality Based on a Quality Assurance Score System in the Bohai Sea

Xiaoyan Liu [1,2,3], Qian Yang [4], Yunhua Wang [1] and Yu Zhang [2,*]

[1] Faculty of Information Science and Engineering, Ocean University of China, Qingdao 266100, China; liuxiaoyan@qlu.edu.cn (X.L.); yunhuawang@ouc.edu.cn (Y.W.)
[2] School of Mathematical Sciences, Ocean University of China, Qingdao 266100, China
[3] Institute of Oceanographic Instrumentation, Qilu University of Technology (Shandong Academy of Sciences), Qingdao 266100, China
[4] College of Ocean Science and Engineering, Shandong University of Science and Technology, Qingdao 266590, China; qianyang@sdust.edu.cn
* Correspondence: zhangyu6929@ouc.edu.cn

Abstract: In the application of ocean color remote sensing, remote sensing reflectance spectral ($R_{rs}(\lambda)$) is the most important and basic parameter for the development of bio-optical algorithms. Atmospheric correction of ocean color data is a key factor in obtaining accurate water $R_{rs}(\lambda)$ data. Based on the QA (quality assurance) score spectral quality evaluation system, the quality of $R_{rs}(\lambda)$ spectral of GOCI (Geostationary Ocean Color Imager) obtained from four atmospheric-correction algorithms in the Bohai Sea were evaluated and analyzed in this paper. The four atmospheric-correction algorithms are the NASA (National Aeronautics and Space Administration) standard near-infrared atmospheric-correction algorithm (denoted as Seadas—Default), MUMM (Management Unit of the North Sea Mathematical Models, denoted as Seadas—MUMM), and the standard atmospheric-correction algorithms of KOSC GOCI GDPS2.0 (denoted as GDPS2.0) and GDPS1.3 (denoted as GDPS1.3). It is shown that over 90% of the $R_{rs}(\lambda)$ data are in good quality with a score $\geq 4/6$ for the GDPS1.3 algorithm. The probability of $R_{rs}(\lambda)$ with a QA score of 1 is significantly higher for the GDPS1.3 algorithm (57.36%), compared with Seadas—Default (37.91%), Seadas—MUMM (35.96%), and GDPS2.0 (33.05%). The field and MODIS measurements of $R_{rs}(\lambda)$ were compared with simultaneous GOCI $R_{rs}(\lambda)$, and they demonstrate that the QA score system is useful in evaluating the spectral shape of $R_{rs}(\lambda)$. The comparison results indicate that higher QA scores have higher accuracy of the R_{rs} band ratio. The QA score system is helpful to develop and evaluate bio-optical algorithms based on the band ratio. The hourly variation of QA score from UTC 00:16 to 07:16 was investigated as well, and it demonstrates that the data quality of GOCI $R_{rs}(\lambda)$ can vary in an hour scale. The GOCI data with high quality should be selected with caution when studying the hourly variation of biogeochemical properties in the Bohai Sea from GOCI measurements.

Keywords: remote sensing reflectance; GOCI; QA score; Bohai Sea; atmospheric correction

Citation: Liu, X.; Yang, Q.; Wang, Y.; Zhang, Y. Evaluation of GOCI Remote Sensing Reflectance Spectral Quality Based on a Quality Assurance Score System in the Bohai Sea. *Remote Sens.* **2022**, *14*, 1075. https://doi.org/10.3390/rs14051075

Academic Editors: Cédric Jamet, Seunghyun Son and Youngje Park

Received: 17 December 2021
Accepted: 18 February 2022
Published: 22 February 2022

1. Introduction

With the development of ocean color remote sensing, satellite sensors with high sampling frequency and high space coverage play an important role in studying the bio-optical properties and biogeochemical parameters of seawater [1]. For the coastal water areas with complex bio-optical properties, the diurnal variation dynamics are relatively high due to the complex components, such as phytoplankton, suspended particles, and Chromophoric Dissolved Organic Matter (CDOM) [2]. For a long time, the major ocean color observation sensors were mounted on polar-orbiting satellites, such as SeaWiFS (Sea-viewing Wide Field Sensor), MODIS (Moderate-Resolution Imaging Spectroradiometer), MERIS

(Medium-Resolution Imaging Spectrometer), VIIRS (Visible Infrared Imager Radiometer Sensor), OLCI (Ocean and Land Color Instrument), and COCTS (Chinese Ocean Color and Temperature Scanner). They all generally covered the world once every 1–2 days or more, which made them unsuitable for studying the temporal and spatial variation of short time series on the coast. COMS (Communication Ocean and Meteorological Satellite), the first geostationary oceanic satellite of the world, was launched in 2010, and GOCI (Geostationary Ocean Color Imager) is the main sensor on it [3]. Compared with traditional polar-orbiting ocean water color satellites, the GOCI can provide 8 observations per day, while the second GOCI(GOCI-II) can provide 10, making it possible to observe hourly variations in biogeochemical parameters [4]. In addition, it can help monitor short-term changes in water quality, red tides, green tides, etc., in the nearshore waters [5,6]. Recently, many researchers used GOCI data to retrieve water environmental parameters, such as chlorophyll, suspended particle matter (SPM), water transparency, CDOM, sea ice, etc. [7–11].

The so-called spectral remote sensing reflectance $R_{rs}(\lambda)$ data of waters are defined as the ratio of water-leaving radiance to downwelling irradiance above the sea surface, and are a crucial parameter to retrieve optical properties and biogeochemical parameters of seawater. For ocean color remote sensing, about 90% of the total signal received by the sensor is contributed from the atmosphere, while the water-leaving radiance of seawater contributes less than 10%. Therefore, atmospheric correction is preformed firstly to remove the atmospheric signals and obtain water-leaving radiance or $R_{rs}(\lambda)$ [12]. Gordon et al. proposed an atmospheric-correction algorithm for clear oceanic waters, where the assumption of zero water-leaving radiance at the NIR bands is valid (also known as 'black-pixel') [13]. However, this black-pixel assumption is invalid for turbid case-2 water bodies [14–18]. To counter this, some researchers proposed several atmospheric-correction algorithms which account for the fact that the water-leaving radiance of case-2 water bodies is not zero in the NIR bands. These algorithms can be summarized as follows: (1) use of SWIR bands [17,19,20] or use of blue or UV bands [21,22]; (2) assuming/modeling the contributions of NIR aerosol or water [18,23–27]; (3) correcting/modeling of the non-negligible ocean in the NIR [14,28,29]; (4) based on a neural network method [30–32] or optimization method [33–35]. The traditional and commonly used method for evaluating the quality of ocean color data (including $R_{rs}(\lambda)$ data) is to compare the satellite measurements with field measurements with statistical analysis. This provides important information on the overall quality of various ocean color observation data [36–40]. However, it has been shown that the actual meaning of the single band contrast scatter plot cannot clearly express the quality of the complete $R_{rs}(\lambda)$ spectrum [36,39]. Many bio-optical algorithms are based on the $R_{rs}(\lambda)$ spectrum to derive biogeochemical parameters, such as the band ratio algorithm for chlorophyll concentration, which requires more precise quality assurance of the full $R_{rs}(\lambda)$ spectrum [41,42]. Wei et al. [43] established a QA (quality assurance) system that could objectively evaluate the spectral quality of $R_{rs}(\lambda)$ based on large numbers of high-quality field hyperspectral reflectance data. It could objectively evaluate the spectral quality of $R_{rs}(\lambda)$. A further test on the QA system used the NOMAD (NASA bio-Optical Marine Algorithm Dataset) remote sensing reflectance dataset and satellite remote sensing reflectance data from coastal and oceanographic regions. The results show that the QA evaluation system can identify problems or possibly erroneous $R_{rs}(\lambda)$ spectra.

GDPS (GOCI Data Processing System) is a data analysis and processing software specially designed for GOCI sensor data. The development of the initial version of GDPS began in 2003 and was completed in 2008. GDPS provides two different modes of operation: the server (real-time) mode, which is used at the GOCI data-processing facility for real-time generation of oceanic color data and information, and the interactive mode, which is open to the scientific community. Up to now, Korea Ocean Satellite Center (KOSC) has provided GDPS1.1, GDPS1.2, GDPS1.3, GDPS1.4, GDPS1.4.1, and GDPS2.0 for global

users [3,27,44,45]. Recently, NASA's SeaDAS software also included specific modules to process GOCI's data, making the application of alternative processing algorithms easy [46–48].

GOCI's frequent measurements provide an important data source for the monitoring and research of daily changes in water quality. The evaluation and analysis of GOCI $R_{rs}(\lambda)$ spectral quality are also particularly important. In this study, the QA score system is used to evaluate the GOCI $R_{rs}(\lambda)$ spectrum in the Bohai Sea. We select four atmospheric-correction algorithms, the default atmospheric-correction algorithm by SeaDAS (denoted by Seadas—Default in this study), MUMM (denoted by Seadas—MUMM), the standard atmospheric-correction algorithms of KOSC GDPS2.0 (denoted by GDPS2.0), and GDPS1.3 (denoted by GDPS1.3) to process GOCI L1B data to generate $R_{rs}(\lambda)$ spectrum. The QA scores of the four algorithms are calculated. Then, the GOCI $R_{rs}(\lambda)$ are compared with in situ and MODIS measurements to analyze the QA score system in evaluating the $R_{rs}(\lambda)$ spectrum in the Bohai Sea and the quality of the $R_{rs}(\lambda)$ spectrum from different algorithms. At last, the hourly variation of GOCI $R_{rs}(\lambda)$ QA score from UTC 00:16 to 07:16 is analyzed.

2. Data and Algorithm

2.1. Study Area

This study is focused on the Bohai Sea, China's northernmost coastal waters, which is a nearly enclosed inland sea. According to topography and landforms, the Bohai Sea can be divided into five parts: Liaodong Bay, Bohai Bay, Laizhou Bay, Bohai Sea, and Bohai Strait (Figure 1). This sea area is the confluence of many rivers, including the famous Yellow River. Bohai Strait is the only channel for the exchange of water in the Bohai Sea with the Yellow Sea. The surrounding coastal land area is called the Bohai Rim Economic Circle; it is characterized by intense human activity, causing the rapid degradation of the Bohai Sea's ecosystem and a decline in primary productivity [49]. The real-time dynamic monitoring of the water quality and ecological conditions of this complex sea area is thus of great significance.

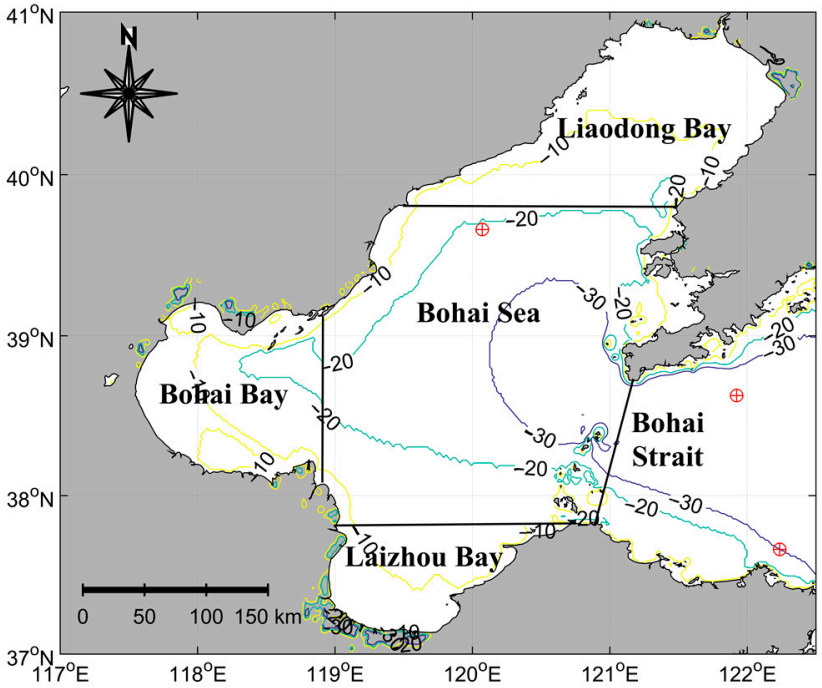

Figure 1. The map of Bohai Bay, Laizhou Bay, Liaodong Bay, Bohai Sea, and Bohai Strait. The red dots indicate the field experimental station used in this study.

2.2. Data

2.2.1. GOCI Data

GOCI is the main sensor on South Korea's COMS Satellite. Launched in July 2010, COMS is the world's first geostationary ocean color satellite. It covers China's Bohai Sea, Yellow Sea, and parts of the East China Sea and captures eight images per day from 8 am to 3 pm in local time, one image per hour. The sweep width of the GOCI image is 2500 km × 2500 km, the orbital altitude is 35,837 km, the spatial resolution is 500 m, and the band range is 412–865 nm (6 visible bands and 2 near-infrared bands, as shown in Table 1). The GOCI L1B data of 27 August 29 to 2015, and September 2015, with a total of 264 images, were used in this paper, as obtained from: http://kosc.kiost.ac.kr/, accessed on 15 June 2021.

2.2.2. MODIS/Aqua Data

Aqua is a solar synchronous polar-orbiting satellite. Moderate-resolution Imaging Spectroradiometer (MODIS) is one of the main sensors mounted on Aqua. Its sweep width is 2330 km, its spectral band range is 140–1440 nm, and it has 36 spectral bands. In this paper, Aqua MODIS L2 daily R_{rs} data of September 2015, with a total of 30 images, were applied. We obtained those MODIS R_{rs} data from the NASA Ocean Biology Processing Group (OBPG, http://oceancolor.gsfc.nasa.gov/, accessed on 15 June 2021), which were processed with the most recent updates in calibration and algorithms.

Bands settings of GOCI and MODIS are as follows (Table 1).

Table 1. Common bands of MODIS and GOCI.

Band	MODIS Wavelength (nm)	Band	GOCI Wavelength (nm)
1	412	1	412
2	443	2	443
3	469	3	490
4	488	4	555
5	531	5	660
6	547	6	680
7	555	7	745
8	667	8	865
9	678		
10	748		
11	859		
12	869		

2.2.3. In Situ Data

From 27 to 29 August 2015, we conducted an in situ experiment of Marine optics in the Yellow Sea and Bohai Sea. The upward radiance profile data and downward irradiance profile data were measured with a hyperspectral radiometer, Profiler II, whose manufacturer is Satlantic. Its downward irradiance data, $E_d(\lambda, z)$, and upward radiance data, $L_u(\lambda,z)$, can be expressed as:

$$E_d(\lambda, z) = E_d(\lambda, 0^-) \exp[K_d(\lambda) \times z] \quad (1)$$

$$L_u(\lambda, z) = L_u(\lambda, 0^-) \exp[K_L(\lambda) \times z] \quad (2)$$

where $E_d(\lambda, 0^-)$ and $L_u(\lambda, 0^-)$ are the downward irradiance and upward radiance just below the sea surface, respectively. $K_d(\lambda)$ and $K_L(\lambda)$ are diffuse attenuation coefficients of downward irradiance and upward radiance, respectively. According to Equations (1) and (2), the measured data of $E_d(\lambda, z)$ and $L_u(\lambda, z)$ were fitted to obtain $E_d(\lambda, 0^-)$, $L_u(\lambda, 0^-)$, $K_d(\lambda)$, and $K_L(\lambda)$. Then, $R_{rs}(\lambda)$ can be obtained by Equation (3) [1].

$$\mathrm{rrs}(\lambda) = L_u(\lambda, 0^-)/E_d(\lambda, 0^-), R_{rs}(\lambda) = 0.52 \times \mathrm{rrs}(\lambda)/(1 - 1.7 \times \mathrm{rrs}(\lambda)) \quad (3)$$

2.3. Algorithm

2.3.1. Atmospheric-Correction Algorithms of GDPS

The operational algorithm of atmospheric correction for GDPS to process GOCI data adopts the bright pixel method, which is implemented by improving the iterative model for calculating NIR water-leaving reflectance based on the standard SEAWIFS algorithm. Because of the absence of SWIR band in GOCI, GDPS1.3 used the empirical relation between the red band and NIR water-leaving reflectance to calculate the NIR reflectance ρ_w (Equations (4) and (5)) [44]. GDPS1.4 mainly updates the modularization of the software based on GDPS1.3 and fixes some minor problems of modularization. The atmospheric-correction algorithm of GDPS1.3 and GDPS1.4 are identical, and the $R_{rs}(\lambda)$ obtained from them were the same [44].

$$\rho_w(745) = \sum_{n=1}^{6} j_n \rho_w^n(660) \tag{4}$$

$$\rho_w(865) = \sum_{n=1}^{2} k_n \rho_w(745) \tag{5}$$

The atmospheric correction of GDPS2.0 makes use of the SRAMS (spectral relationships in the aerosol multiple-scattering reflectance) among different wavelengths to directly calculate the contribution of near-infrared multiple-scattering reflectance. Then, the reflectance contribution of the near-infrared band to the visible band of the aerosol model is estimated by the SRAMS spectrum [27]. The spectral relation between the reflection spectra of multi-scattered aerosols and different wavelengths is established by a polynomial function (Equation (6)):

$$\rho_w(\lambda_2) = \sum_{n=1}^{D} c_n \rho_w^n(\lambda_1) \tag{6}$$

For GOCI data, the spectral relations of each GOCI spectral segment are summarized in Table 2. D represents the calculation order.

Table 2. Spectral relations of each GOCI spectral band.

λ_1 (nm)	555	555	555	745	745	745	865
λ_2 (nm)	412	430	490	555	660	680	745
D	4	4	4	4	3	3	2

Compared with the atmospheric-correction algorithm of GDPS1.1 and GDPS1.2, GDPS1.3 adds the calculation order of the empirical relation of the water-leaving reflectance. The atmospheric-correction algorithm of GDPS2.0 is different from the previous version. Then, the default atmospheric-correction algorithms of GDPS1.3 and GDPS2.0 were used in this paper to conduct atmospheric correction on GOCI L1B data. The corrected remote sensing reflectance spectral ($R_{rs}(\lambda)$) data were obtained.

2.3.2. Atmospheric-Correction Algorithms of SeaDAS

SeaDAS provides a variety of atmospheric-correction algorithms for users in the atmospheric correction of remote sensing data. In this paper, the default atmospheric-correction algorithm of SeaDAS 7.5 (i.e., NASA standard atmospheric-correction algorithm, denoted as Seadas—Default in this paper) and MUMM atmospheric-correction algorithm (denoted as Seadas—MUMM in this paper) are used to conduct atmospheric correction on GOCI data. Then, we can obtain the corrected remote sensing reflectance spectral ($R_{rs}(\lambda)$) data.

The default atmospheric-correction algorithm for SeaDAS was originally developed by Gordon and Wang [13] in 1994, and in 2003, Stumpf et al. [28] extended its application to case-2 waters. Bailey et al. revised it in 2010, also exhibiting good performances for complex optical water bodies [50]. This algorithm assumes that the remote sensing reflectance with the removal of the reflection of atmospheric molecules is either only related to aerosols or only related to waters. First, ρ_w at 443 nm, 490 nm, and 555 nm are retrieved based on the black-pixel assumption. Then, based on the bio-optical model (Equation (7)), the absorption of particles and CDOM in the red band is determined. Additionally, the particulate backscattering in the red band and NIR band can be computed. At last, ρ_w in the NIR bands are generated.

$$\rho_w(\lambda) = f(\lambda, \mathrm{Chl}) \tag{7}$$

The MUMM atmospheric-correction algorithm was proposed by Ruddick in 2000 [24]. The assumptions of this algorithm consist of two parts:

(1) The aerosol multiple-scattering reflectance ratio of the two near-infrared bands of each pixel has a fixed value, defined as ε(745,865), then:

$$\varepsilon(745, 865) = \frac{\rho_A(745)}{\rho_A(865)}, \tag{8}$$

where ρ_A includes both Rayleigh and aerosol scatterings, as well as the interaction between them.

(2) The ratio between reflectance and atmospheric transmission at the two near-infrared bands (α(745,865)) is constant and equal to 1.945.

$$\alpha(745, 865) = \frac{\rho_w(745)/t(745)}{\rho_w(865)/t(865)} = 1.945, \tag{9}$$

where ρ_w is the water-leaving reflectance, and t is the diffuse transmittance from the sun to the ocean atmosphere.

Then, using the set value of α and the estimated values of ε, Equations (10) and (11) are defined. The values of $\rho_A(745)$ and $\rho_A(865)$ are estimated to select appropriate aerosol models. Finally, the aerosol models are reentered into the black-pixel assumption, and ρ_w data are obtained.

$$\rho_A(865) = \frac{\alpha\rho_{rc}(865) - \rho_{rc}(745)}{\alpha - \varepsilon(745, 865)} \tag{10}$$

$$\rho_A(745) = \varepsilon(745, 865)\left(\frac{\alpha\rho_{rc}(865) - \rho_{rc}(745)}{\alpha - \varepsilon(745, 865)}\right) \tag{11}$$

2.3.3. QA Score System

QA score system is based on the clustering analysis of optical water types, which is also the core point of the QA system. The steps for the establishment and application of the QA system are as follows:

Firstly, the reference R_{rs} spectra were normalized by their respective root of the sum of squares to obtain nR_{rs}.

$$nR_{rs}(\lambda) = \frac{R_{rs}(\lambda)}{\left[\sum_{i=1}^{N} R_{rs}(\lambda_i)^2\right]^{1/2}} \tag{12}$$

where N represents the total number of wavelengths equal to 9. λ_i corresponds to the wavelengths of 412, 443, 488, 510, 531, 547, 555, 667, and 678 nm. The nR_{rs} spectra vary over the range between 0 and 1, while they retain the 'shapes' pertaining to the original

R_{rs} spectra, i.e., the band ratios of $nR_{rs}(\lambda)$ remain the same as $R_{rs}(\lambda)$. If the $R_{rs}(\lambda)$ data were measured at other wavelengths, it is needed to find the closest wavelength from the nine bands. Finally, the gap method was used to determine the optimal number of clustering k = 23, which was exactly consistent with the number of optical water types.

Secondly, we obtained the spectra of normalized remote sensing reflectance of 9 bands of 23 kinds of optical waters. Through the nR_{rs} spectrum, the upper boundary and lower boundary values of each band's nR_{rs} spectrum of each water can be obtained, as well as the average value of the nR_{rs} spectrum. Thus, the average value of the nR_{rs} spectrum, the upper boundary of the nR_{rs} spectrum, ${nR_{rs}}^{U}$, and the lower boundary of the nR_{rs} spectrum, ${nR_{rs}}^{L}$, form the key part of the QA evaluation system [43].

Thirdly, we can give a target $R_{rs}^{*}(\lambda')$ and evaluate it with the QA system. First, we must figure out whether the target $R_{rs}^{*}(\lambda')$ band matches that of $nR_{rs}(\lambda)$. If the spectral bands of $R_{rs}^{*}(\lambda')$ are more than those of $nR_{rs}(\lambda)$, only the bands with the same wavelength as $nR_{rs}(\lambda)$ are selected for further analysis. If the spectral bands of $R_{rs}^{*}(\lambda')$ are fewer than those of $nR_{rs}(\lambda)$ (i.e., the total number of bands is less than nine), the $nR_{rs}(\lambda')$ subset corresponding to λ' and the corresponding ${nR_{rs}}^{U}(\lambda')$ subset and ${nR_{rs}}^{L}(\lambda')$ subset need to be extracted from $nR_{rs}(\lambda)$. Then, $nR_{rs}^{*}(\lambda')$ is obtained after the normalization of $R_{rs}^{*}(\lambda')$ with Equation (12). According to the similarity equation of SAM spectrum proposed by Kruse [51] (Equation (13)), we can assign a water type for $nR_{rs}^{*}(\lambda')$.

$$\cos\alpha = \frac{\sum_{i=1}^{N}\left[nR_{rs}^{*}(\lambda)\cdot nR_{rs}(\lambda)\right]}{\sqrt{\sum_{i=1}^{N}\left[nR_{rs}^{*}(\lambda_{\,i})\right]^{2}\sum_{i=1}^{N}\left[nR_{rs}(\lambda_{\,i})\right]^{2}}} \tag{13}$$

where α is the angle formed between the reference spectrum, nR_{rs}, and the normalized target spectrum, nR_{rs}^{*}. SAM can determine the spectral similarity by taking them as the space vector whose dimension is equal to the band number N, and the spectral water type corresponding to the maximum cosine value is determined as the water type of the target spectrum, nR_{rs}^{*}.

Finally, the QA score is estimated by comparing the upper and lower boundary values of the target spectrum nR_{rs}^{*} with the spectra of water types (Equation (14)).

$$C_{\mathrm{tot}} = \frac{C(\lambda_1) + C(\lambda_2) + \ldots + C(\lambda_N)}{N} \tag{14}$$

$C(\lambda_i)$ is the score for a particular wavelength, and N is the total number of bands in nR_{rs}^{*}. If the value of $nR_{rs}^{*}(\lambda_i)$ is not in the range of ${nR_{rs}}^{U}(\lambda_i)$ and ${nR_{rs}}^{L}(\lambda_i)$, the wavelength score will be assigned 0, that is, $C(\lambda_i) = 0$; otherwise, $C(\lambda_i) = 1$. As can be seen from Equation (14), the total score of nR_{rs}^{*} varies within the range of [0, 1]. Additionally, a higher score means better data quality.

3. Results

3.1. Statistical Analysis of the $R_{rs}(\lambda)$ QA Score

The total QA score of all the six GOCI bands is expressed as $n/6$ (n = 0,1,2,3,4,5,6), and n is the total number of bands where the score of the specific band is 1. Figure 2 shows the frequency distribution of GOCI $R_{rs}(\lambda)$ QA scores in the Bohai Sea in Sep. 2015, obtained from the atmospheric-correction algorithms of Seadas—Default, Seadas—MUMM, GDPS2.0, and GDPS1.3, and Table 3 lists the values of the frequencies. More than 48 million data were counted, with about 12.2+ million available pixels for Seadas—Default, 12.2+ million available pixels for Seadas—MUMM, 11.7+ million available pixels for GDPS2.0, and 11.8+ million available pixels for GDPS1.3. It can be seen that the frequency increases with scores, especially for scores from GDPS1.3. A total of 57.36% of the $R_{rs}(\lambda)$ data from the GDPS1.3 has a QA score of 1, while for the other three atmospheric-correction algorithms, less than a half of the $R_{rs}(\lambda)$ data have a score of 1, i.e., 37.91% for Seadas—Default, 35.96%

for Seadas—MUMM, and 33.05% for GDPS2.0. If we take the score of 4/6 (~0.67) as a relatively high score, about 93% of the $R_{rs}(\lambda)$ data are of good quality with a score no less than 4/6 for the GDPS1.3 algorithm. For the other three atmospheric-correction algorithms, about 81–88% of the $R_{rs}(\lambda)$ data has a relatively high quality. Therefore, the frequency distribution of the QA score reveals that GOCI $R_{rs}(\lambda)$ data have good quality in the Bohai Sea, and the atmospheric-correction algorithm embedded in GDPS1.3 is more suitable.

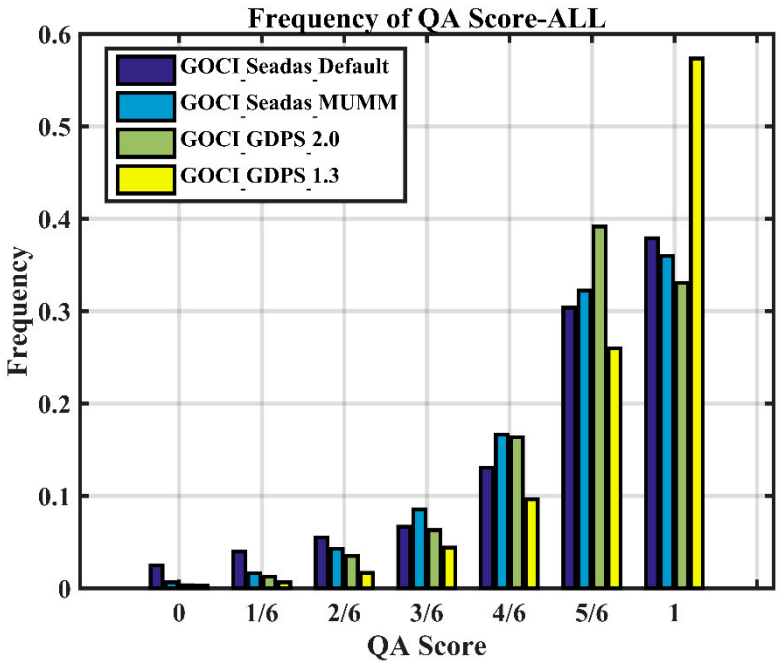

Figure 2. Statistical results of QA score of GOCI $R_{rs}(\lambda)$ data processed by four atmospheric-correction algorithms in the Bohai area.

Table 3. Probability statistical table of QA score distribution of $R_{rs}(\lambda)$ data obtained from each atmospheric-correction algorithm over the whole Bohai area.

QA Score	Frequency			
	Seadas—Default	Seadas—MUMM	GDPS2.0	GDPS1.3
0	2.48%	0.65%	0.34%	0.29%
1/6	3.98%	1.67%	1.28%	0.66%
2/6	5.51%	4.28%	3.50%	1.68%
3/6	6.68%	8.56%	6.32%	4.42%
4/6	13.05%	16.65%	16.36%	9.63%
5/6	30.39%	32.24%	39.17%	25.96%
1	37.91%	35.96%	33.05%	57.36%

The study region is separated into the 'Three Bays' and the 'Bohai Sea' (Figure 1). The Three Bays refers to the Bohai Bay, Liaodong Bay, and Laizhou Bay, where the optical properties of seawater are influenced by human activities. The Bohai Sea refers to the central parts of the region where the seawater is relatively cleaner than the bays. Figure 3 shows the frequency distribution of the QA score at the Three Bays and the Bohai Sea, respectively. Table 4 lists the values of the frequencies. It is obvious that the QA score for the Three Bays is higher than that for the Bohai Sea using any atmospheric-correction algorithm. About 90% of the $R_{rs}(\lambda)$ data has a QA score $\geq$4/6 for the Three Bays, while for the Bohai Sea, only the $R_{rs}(\lambda)$ from GDPS1.3 has about 90% of the data with a score $\geq$4/6. The results indicate the atmosphere correction algorithms are more valid in the coastal areas of the Bohai Sea region.

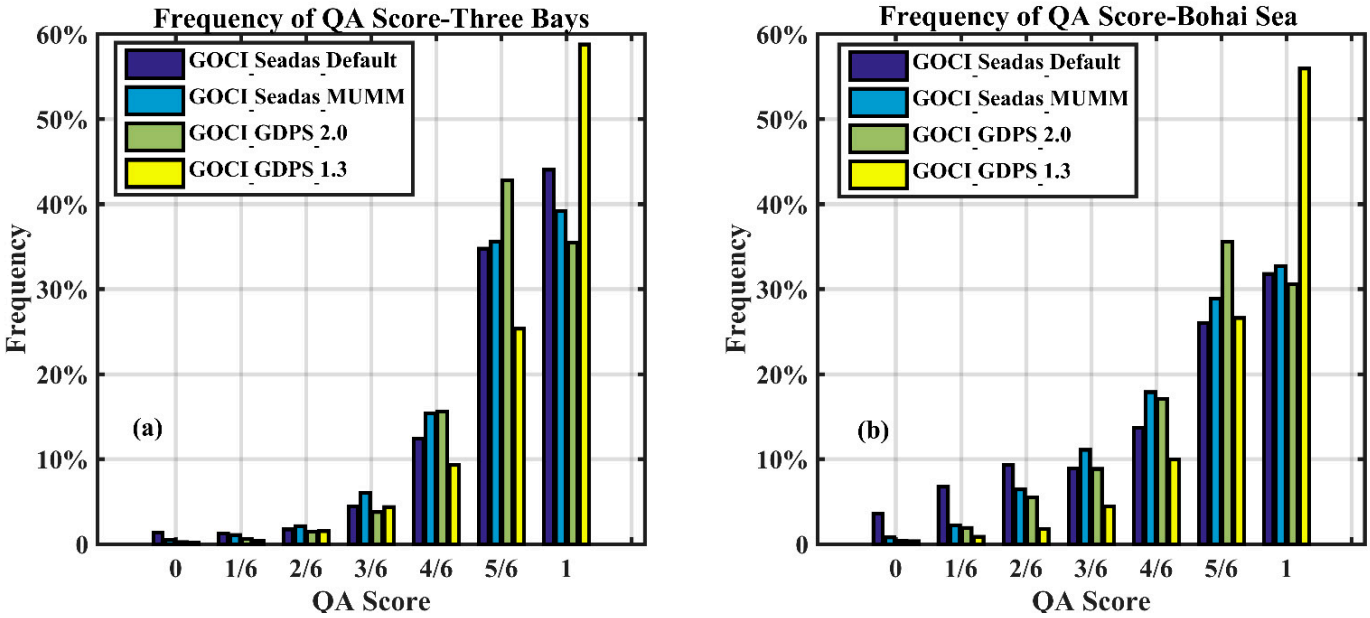

Figure 3. Statistical probability of GOCI $R_{rs}(\lambda)$ QA score of four atmospheric-correction algorithms in each sea area of Bohai Sea. (**a**)Three Bays: Bohai Bay, Liaodong Bay, and Laizhou Bay; (**b**) Bohai Sea.

Table 4. Probability statistical table of QA score distribution of $R_{rs}(\lambda)$ data obtained from each atmospheric-correction algorithm over the different areas of Bohai.

Area	QA Score	Frequency			
		Seadas—Default	Seadas—MUMM	GDPS2.0	GDPS1.3
Three Bays	0	1.36%	0.488%	0.241%	0.22%
	1/6	1.24%	1.100%	0.621%	0.44%
	2/6	1.74%	2.155%	1.474%	1.54%
	3/6	4.45%	6.034%	3.784%	4.39%
	4/6	12.41%	15.407%	15.612%	9.30%
	5/6	34.78%	35.613%	42.780%	25.33%
	1	44.02%	39.203%	35.487%	58.78%
Bohai Sea	0	3.60%	0.81%	0.43%	0.35%
	1/6	6.73%	2.23%	1.94%	0.87%
	2/6	9.28%	6.41%	5.52%	1.82%
	3/6	8.91%	11.08%	8.85%	4.46%
	4/6	13.69%	17.89%	17.10%	9.96%
	5/6	26.00%	28.86%	35.56%	26.60%
	1	31.79%	32.72%	30.60%	55.95%

3.2. Comparison of $R_{rs}(\lambda)$ with Measured In Situ Data

We can consider that the QA score system is developed for evaluating the quality of an individual $R_{rs}(\lambda)$ spectrum. The in situ measurements of $R_{rs}(\lambda)$ were used to compare with GOCI $R_{rs}(\lambda)$ derived from the four atmospheric-correction algorithms with different QA scores. Due to the frequent cloud cover in the study area, the region for the match-up of in situ and GOCI $R_{rs}(\lambda)$ data was extended to the neighboring North Yellow Sea [49]. The spatial and temporal windows of match-up were relaxed to 300 m and 3 h, respectively. Finally, there are seven sets of match-up data in total, and their locations are marked in Figure 1 (red dots). Although the number of match-up data is small, the here is to illustrate the advantage of the QA score system in measuring the spectral shape of GOCI $R_{rs}(\lambda)$, where seven sets of match-ups is acceptable. Three examples of in situ and GOCI $R_{rs}(\lambda)$ spectra are shown in Figure 4 with captions of QA scores. It was found that the spectra shape of the $R_{rs}(\lambda)$ from

GDPS1.3 agrees very well with that of in situ $R_{rs}(\lambda)$, with the highest QA score of 4/6 or 3/6. However, the magnitude of single-band $R_{rs}(\lambda)$ from GDPS1.3 is not always in the best agreement with the in situ data. The QA score is a good indicator for evaluating the spectra shape of $R_{rs}(\lambda)$. This is obviously shown in Figure 4c. The QA scores of the $R_{rs}(\lambda)$ from GDPS1.3 and Seadas—Default are both 4/6, but their magnitudes differ significantly. The $R_{rs}(\lambda)$ from Seadas—Default agrees with the in situ $R_{rs}(\lambda)$ very well.

Since the QA score is more valid in measuring $R_{rs}(\lambda)$ spectra shape, it is interesting to evaluate the band ratio of GOCI $R_{rs}(\lambda)$ by the QA score system. NASA OC2M-HI [42] is a widely used algorithm for retrieving chlorophyll concentration, using the band ratio of $R_{rs}(469)/R_{rs}(555)$. Figure 5 exhibits the values of GOCI and in situ match-up R_{rs} at 469 and 555 nm, as well as the values of the band ratio. Because GOCI does not have a band similar to the wavelength of 469 nm, the value of $R_{rs}(469)$ was generated by a linear interpolation model from the existing GOCI bands. Table 5 shows the averaged unbiased percentage difference ε, which is defined as Equation (15), the root mean square error RMSE, and the average QA score. It is clear that although the values of GOCI $R_{rs}(\lambda)$ at 469 and 555 nm from GDPS1.3 (Figure 5 red circles) do not agree well with the in situ data (black circles), the value of the band ratio $R_{rs}(469)/R_{rs}(555)$ is close to the value of in situ data. As seen from Table 5, for GDPS1.3, the value of ε is 59.26% and 51.01% for $R_{rs}(469)$ and $R_{rs}(555)$, respectively, while the value of $R_{rs}(469)/R_{rs}(555)$ decreases to 10.34%. Accordingly, the average value of the QA score of GDPS1.3 is the highest, i.e., ~0.64. The GDPS2.0 algorithm generates the lowest QA score of $R_{rs}(\lambda)$, i.e., ~0.31, and the percentage difference ε of the band ratio $R_{rs}(469)/R_{rs}(555)$ between the in situ and GDPS2.0 is the largest, i.e., 43.04%. However, for a single wavelength, the ε between the in situ and GOCI $R_{rs}(\lambda)$ from GDPS2.0 is the smallest, i.e., 15.84% at 555 nm. Therefore, if the band ratio of $R_{rs}(\lambda)$ spectrum needs to be applied in the development of the bio-optical algorithm, it is suggested to carry out comprehensive quality evaluation using the QA score system to select the most suitable atmospheric-correction algorithm.

$$\varepsilon = \frac{1}{n} \cdot \sum_{1}^{n} \left[R_{rs\text{-}goci} - R_{rs\text{-in\_}situ} \right] / \left[R_{rs\text{-}goci} + R_{rs\text{-in\_}situ} \right] * 200\% \quad (15)$$

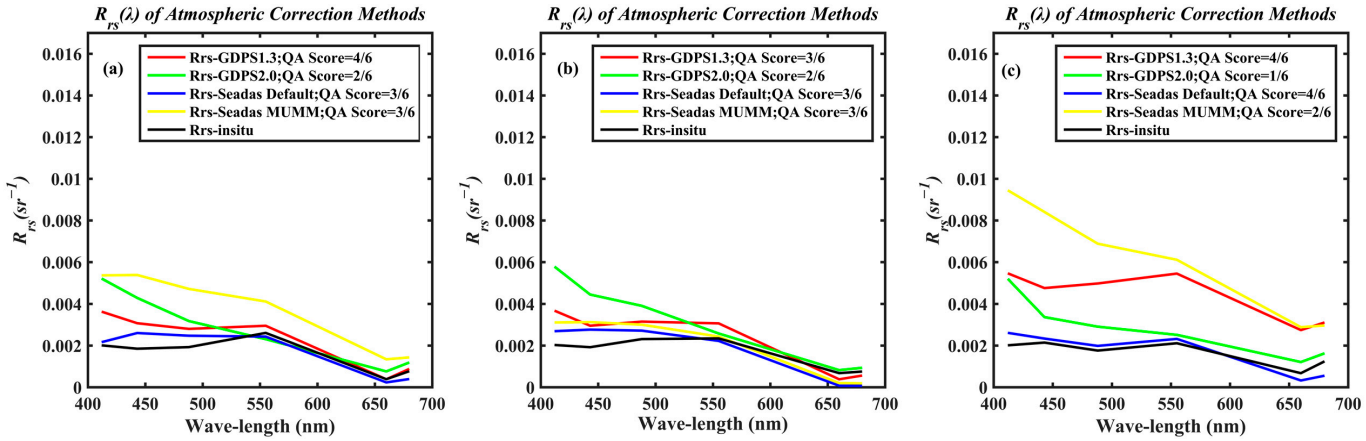

Figure 4. GOCI $R_{rs}(\lambda)$ spectra obtained from four atmospheric-correction algorithms versus in situ $R_{rs}(\lambda)$ spectra in the three matched stations. (**a**–**c**) respectively correspond to the three station points in Figure 1.

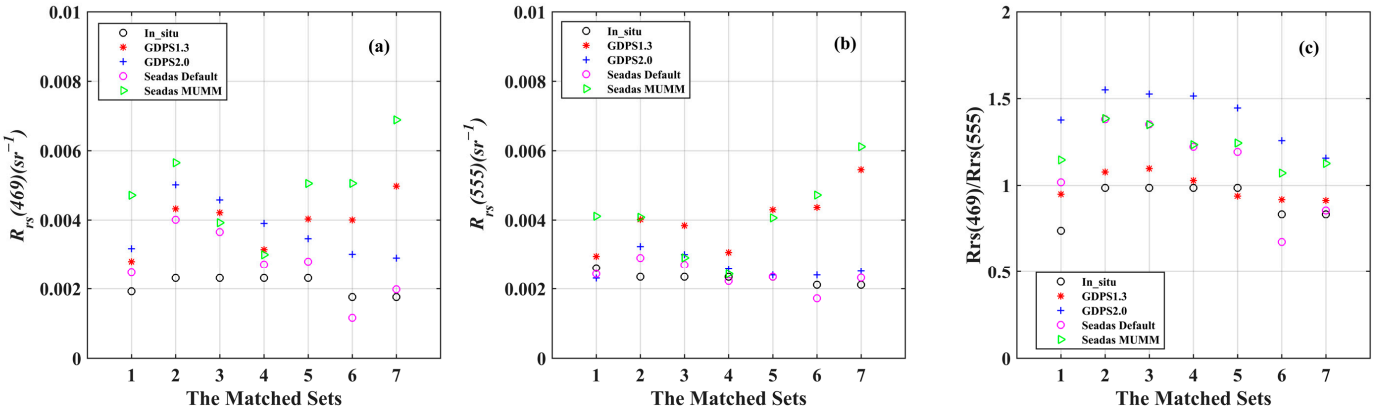

Figure 5. Comparison results between GOCI $R_{rs}(469)$, $R_{rs}(555)$, and $R_{rs}(469)/R_{rs}(555)$ obtained from four atmospheric-correction algorithms and in situ data of the 7 sets of matched data. (**a**) $R_{rs}(469)$; (**b**) $R_{rs}(555)$; (**c**) $R_{rs}(469)/R_{rs}(555)$.

Table 5. The parameter values of the four GOCI atmospheric-correction algorithms in $R_{rs}(469)$, $R_{rs}(555)$, and $R_{rs\text{-}chla} = R_{rs}(469)/R_{rs}(555)$ compared with in situ data.

R_{rs}	Atmospheric Correction Algorithms	ε	RMSE	Mean of QA Score
$R_{rs}(469)$	Seadas—Default	30.31%	0.00091	0.595
	Seadas—MUMM	76.59%	0.00309	0.476
	GDPS2.0	54.59%	0.00172	0.310
	GDPS1.3	59.26%	0.00198	0.643
$R_{rs}(555)$	Seadas—Default	11.13%	0.00031	0.595
	Seadas—MUMM	50.26%	0.00212	0.476
	GDPS2.0	15.84%	0.00048	0.310
	GDPS1.3	51.01%	0.00192	0.643
$R_{rs}(469)/R_{rs}(555)$	Seadas—Default	22.96%	0.26533	0.595
	Seadas—MUMM	29.82%	0.32298	0.476
	GDPS2.0	43.04%	0.50643	0.310
	GDPS1.3	10.34%	0.10863	0.643

3.3. Hourly Variation of the GOCI $R_{rs}(\lambda)$ QA Score from UTC 00:16 to 07:16

The spatial distribution of the GOCI hourly R_{rs} QA score in the Bohai Sea on 13 September 2015 is presented in Figures 6–9 for different atmospheric-correction algorithms. In general, the QA score of GOCI $R_{rs}(\lambda)$ spectral data was extremely lower close to the Bohai Strait, especially for the algorithms of GDPS2.0, Seadas—Default and Seadas—MUMM. The QA score of the R_{rs} generated from GDPS1.3 is high at the eight observation times, except for the data at UTC time 06:16 (Local Time 14:16). Only the score from GDPS2.0 at UTC 06:16 is relatively high. There is a small hourly variation of GOCI spectral quality when we use the atmospheric correction of GDPS2.0. It was noted that the hourly $R_{rs}(\lambda)$ measurement of GOCI at different times has a different spectral quality. The quality of the GOCI $R_{rs}(\lambda)$ spectra exhibits obvious hourly variations for the Seadas—Default and Seadas—MUMM algorithms. In general, the QA score of GOCI $R_{rs}(\lambda)$ is high for the measurements between UTC 02:00 and 04:00. The same characteristic was found in GOCI measurements on 07 September, 19 September, and 20 September 2015 (not shown here).

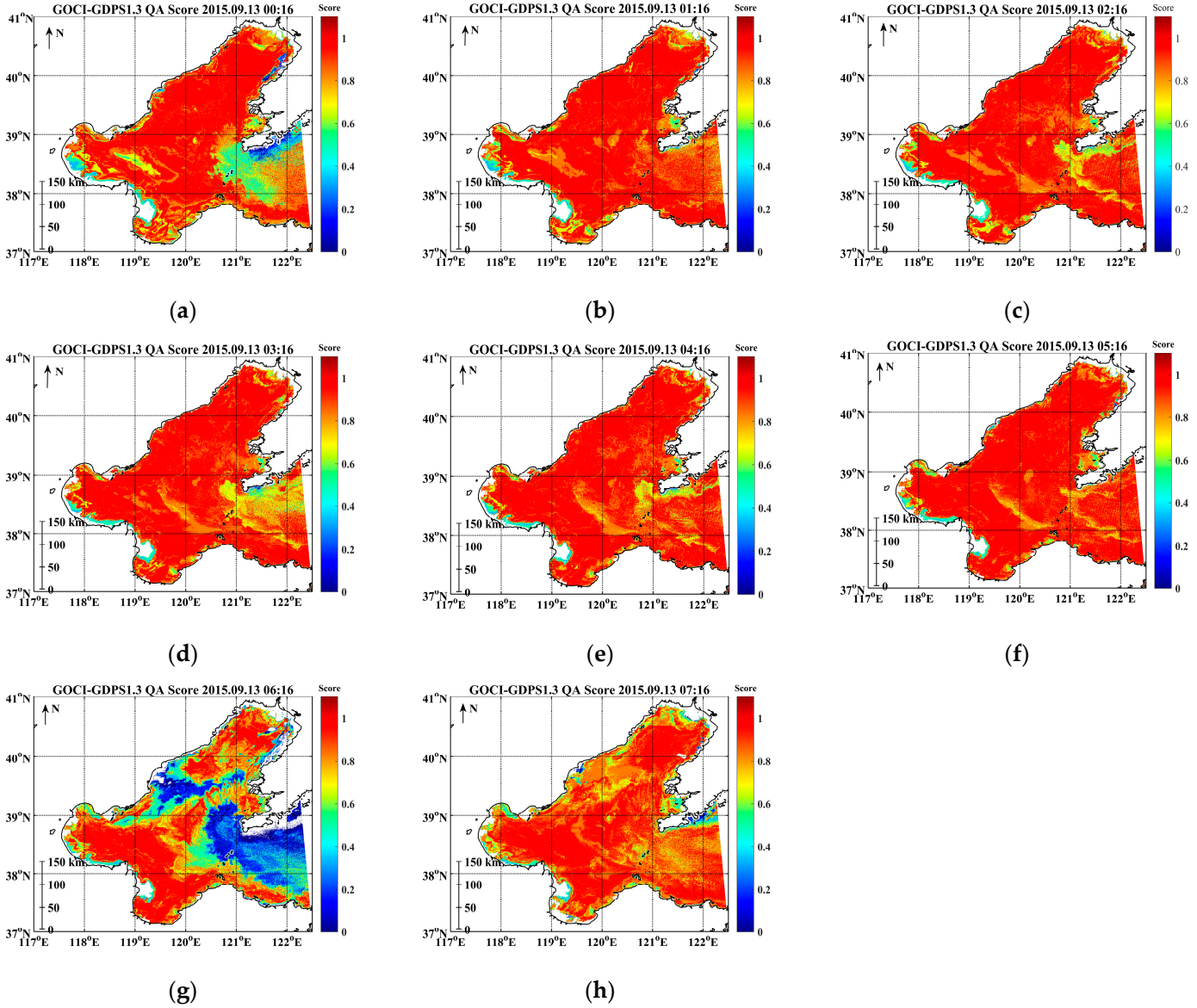

Figure 6. Spatial distribution diagram of GOCI $R_{rs}(\lambda)$ QA score obtained from GDPS1.3—Default atmospheric-correction algorithm on September 13, 2015. (**a**) 00:16; (**b**) 01:16; (**c**) 02:16; (**d**) 03:16; (**e**) 04:16; (**f**) 05:16; (**g**) 06:16; (**h**) 07:16.

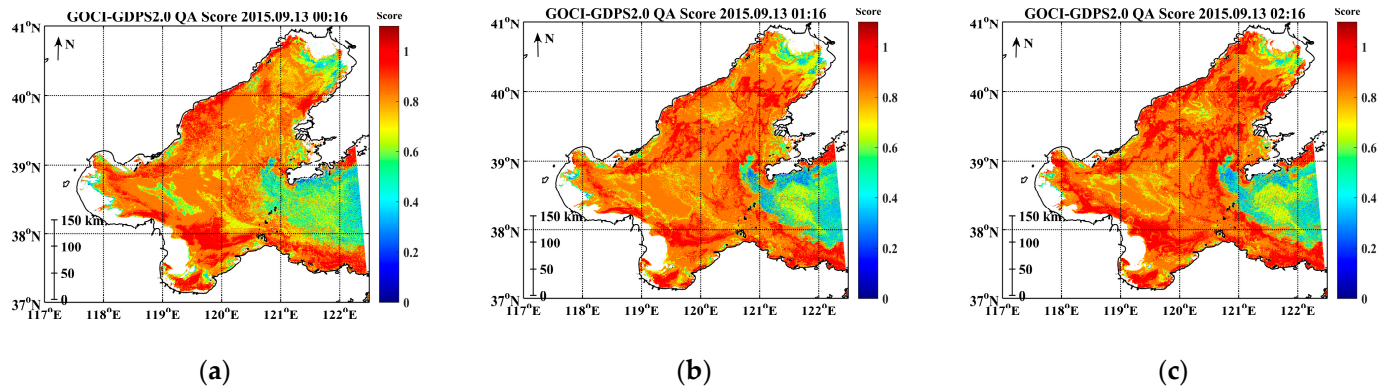

Figure 7. *Cont.*

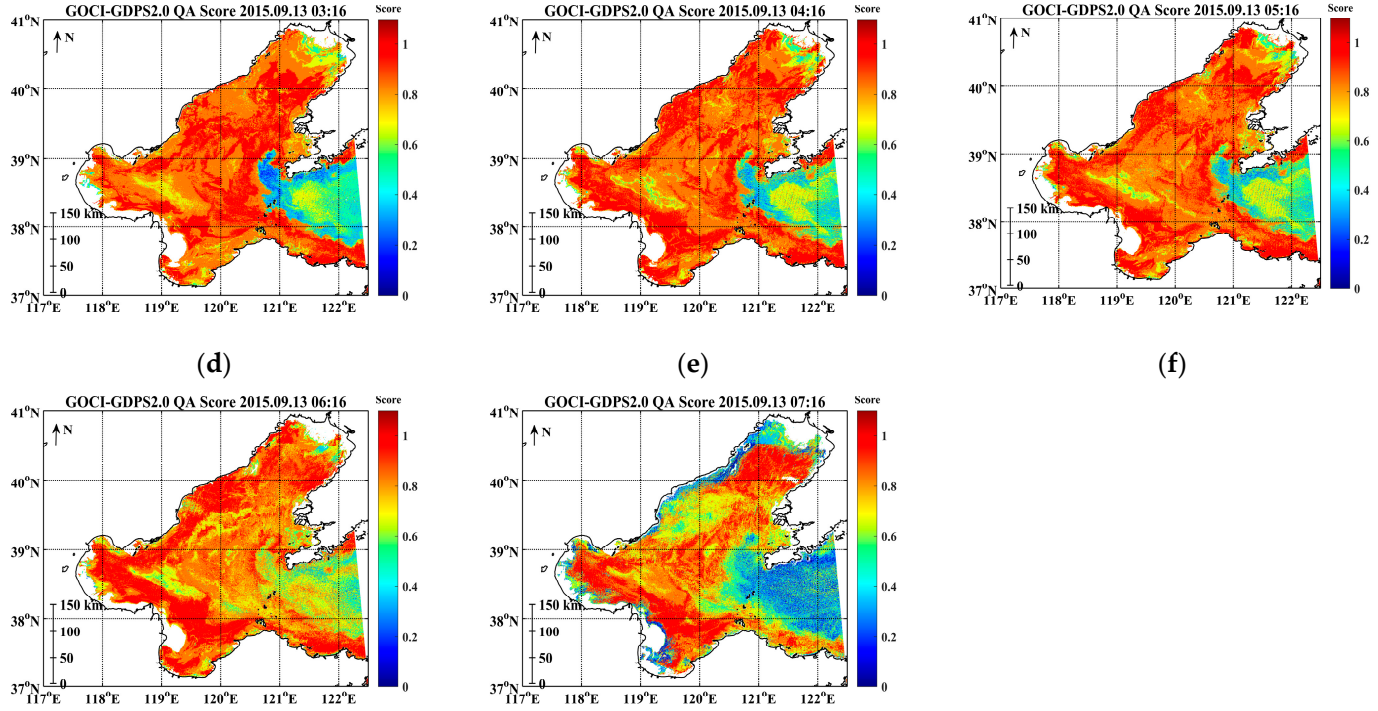

Figure 7. Spatial distribution diagram of GOCI $R_{rs}(\lambda)$ QA score obtained from GDPS2.0—Default atmospheric-correction algorithm on 13 September 2015. (**a**) 00:16; (**b**) 01:16; (**c**) 02:16; (**d**) 03:16; (**e**) 04:16; (**f**) 05:16; (**g**) 06:16; (**h**) 07:16.

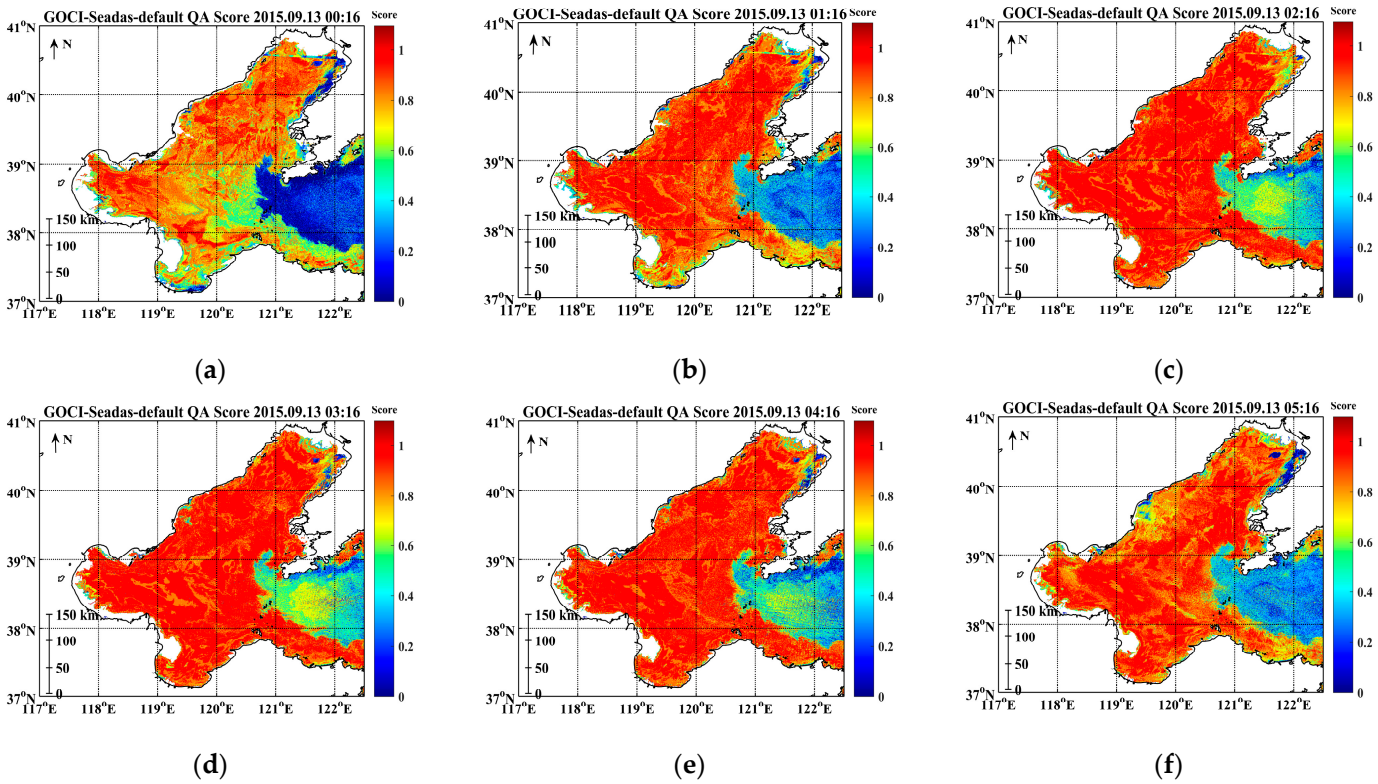

Figure 8. *Cont.*

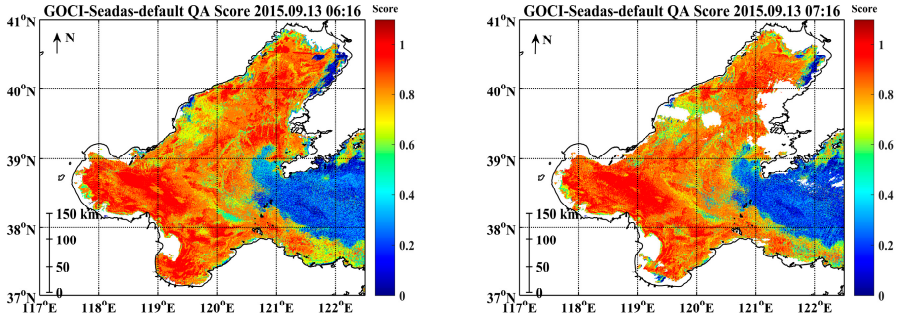

(**g**) (**h**)

Figure 8. Spatial distribution diagram of GOCI $R_{rs}(\lambda)$ QA score obtained from Seadas—Default atmospheric-correction algorithm on 13 September 2015. (**a**) 00:16; (**b**) 01:16; (**c**) 02:16; (**d**) 03:16; (**e**) 04:16; (**f**) 05:16; (**g**) 06:16; (**h**) 07:16.

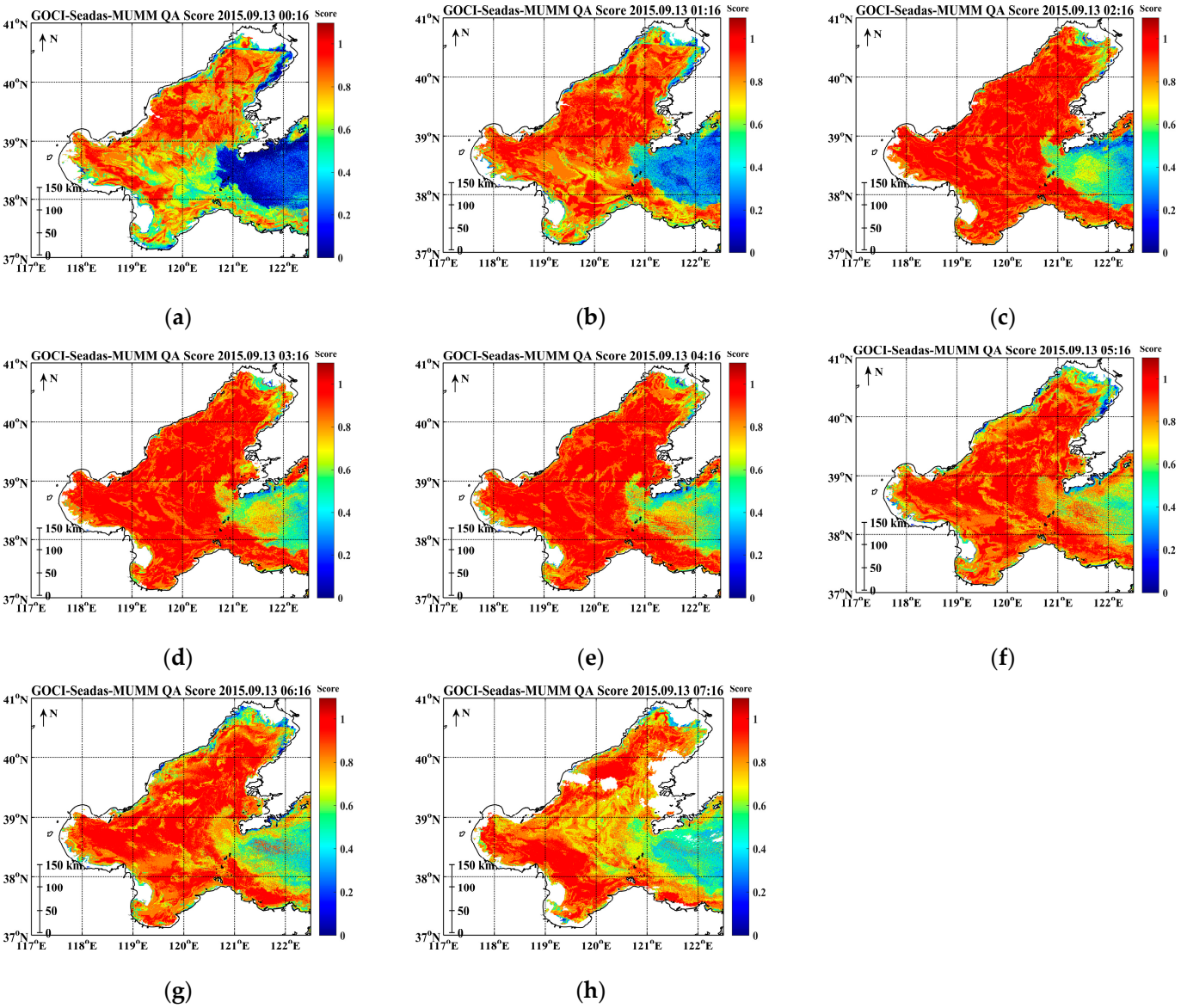

(**a**) (**b**) (**c**)

(**d**) (**e**) (**f**)

(**g**) (**h**)

Figure 9. Spatial distribution diagram of GOCI $R_{rs}(\lambda)$ QA score obtained from Seadas—MUMM atmospheric-correction algorithm on 13 September 2015. (**a**) 00:16; (**b**) 01:16; (**c**) 02:16; (**d**) 03:16; (**e**) 04:16; (**f**) 05:16; (**g**) 06:16; (**h**) 07:16.

Considering that the Bohai Strait plays an important role in the water exchange between the Bohai Sea and the Yellow Sea, its waters' environment and optical properties are more complicated. The QA score of the GOCI $R_{rs}(\lambda)$ spectra obtained by different atmospheric-correction algorithms in the Bohai Strait on 13 September 2015 was calculated. Figure 10 shows the average values of the score at eight observation times. The quality of $R_{rs}(\lambda)$ spectral from GDPS1.3 is good except for the observation at UTC 06:16. The QA scores of $R_{rs}(\lambda)$ from GDPS2.0 are relatively high at the eight observation times. For GDPS2.0 and Seadas MUMM algorithms, the QA scores of $R_{rs}(\lambda)$ obtained by them were relatively consistent from UTC 02:16 to 07:16. When using GOCI measurements for the study of hourly variation from UTC 00:16 to 07:16 in the Bohai Strait, the $R_{rs}(\lambda)$ spectral data derived by GDPS1.3 or GDPS2.0 are helpful.

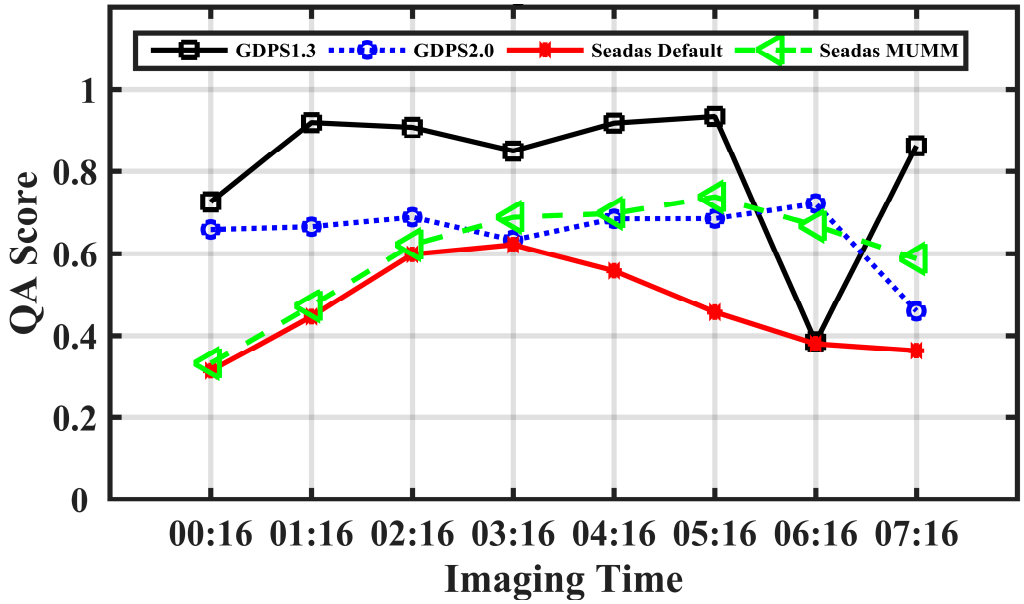

Figure 10. Hourly variations of GOCI $R_{rs}(\lambda)$ QA score from UTC 00:16 to 07:16 in Bohai Strait area on 13 September 2015.

3.4. Cross-Comparison between GOCI and MODIS R_{rs} Data

MODIS data have been extensively used in various ocean studies. Shang et al. [49] validated MODIS $R_{rs}(\lambda)$ data by in situ measurements in the Bohai Sea. They showed that MODIS $R_{rs}(\lambda)$ is in good agreement with the in situ data, with a percentage difference in a range of 9–31% for different bands. In this study, the MODIS L2 product of $R_{rs}(\lambda)$ was used to compare with GOCI $R_{rs}(\lambda)$ for statistical analysis in order to overcome the limitation of fewer in situ measurements.

Only the MODIS $R_{rs}(\lambda)$ data with a QA score of 1 were used here to ensure the spectral quality of MODIS $R_{rs}(\lambda)$. The match-up scheme between MODIS and GOCI data is that the temporal window is no more than 30 min, and the spatial window is no more than 200 m. Finally, a total of 8581 sets of match-up data were obtained in Bohai in September 2015. Figure 11 illustrates the scatter plots of MODIS and GOCI match-ups at 412, 469, and 555 nm, as well as the band ratio of $R_{rs}(469)/R_{rs}(555)$. The MODIS L2 $R_{rs}(\lambda)$ were processed with the default atmospheric-correction algorithm, the same as Seadas—Default for GOCI. The correlation coefficient r, root mean square error RMSE, the defined averaged unbiased percentage difference ε, and the average QA score are given in Tables 6 and 7 for statistical analysis.

As seen in Table 6, the QA scores are high for all four algorithms, i.e., >0.9. Similarly, the errors of band ratio between GOCI and MODIS are also small, ~10% (Table 7). However, Figure 11 and Table 6 show that the error and correlation between GOCI and MODIS R_{rs} are variable with wavelength. For the blue bands, i.e., 412 and 443 nm, the errors

between GOCI and MODIS R_{rs} from the SeaDAS algorithms (Default and MUMM) are relatively smaller than those from the GDPS algorithms (GDPS1.3 and GDPS2.0). The Seadas—Default atmospheric-correction algorithm at 412 nm and 443 nm bands are better than those of the other three algorithms. With a wavelength increase, the relative errors from the GDPS algorithms become smaller. For example, ε is less than 10% for GDPS2.0 and GDPS1.3 at 490, 531, and 555 nm. The correlation between GOCI and MODIS R_{rs} is good except for that from the Seadas—MUMM algorithm at 412 nm.

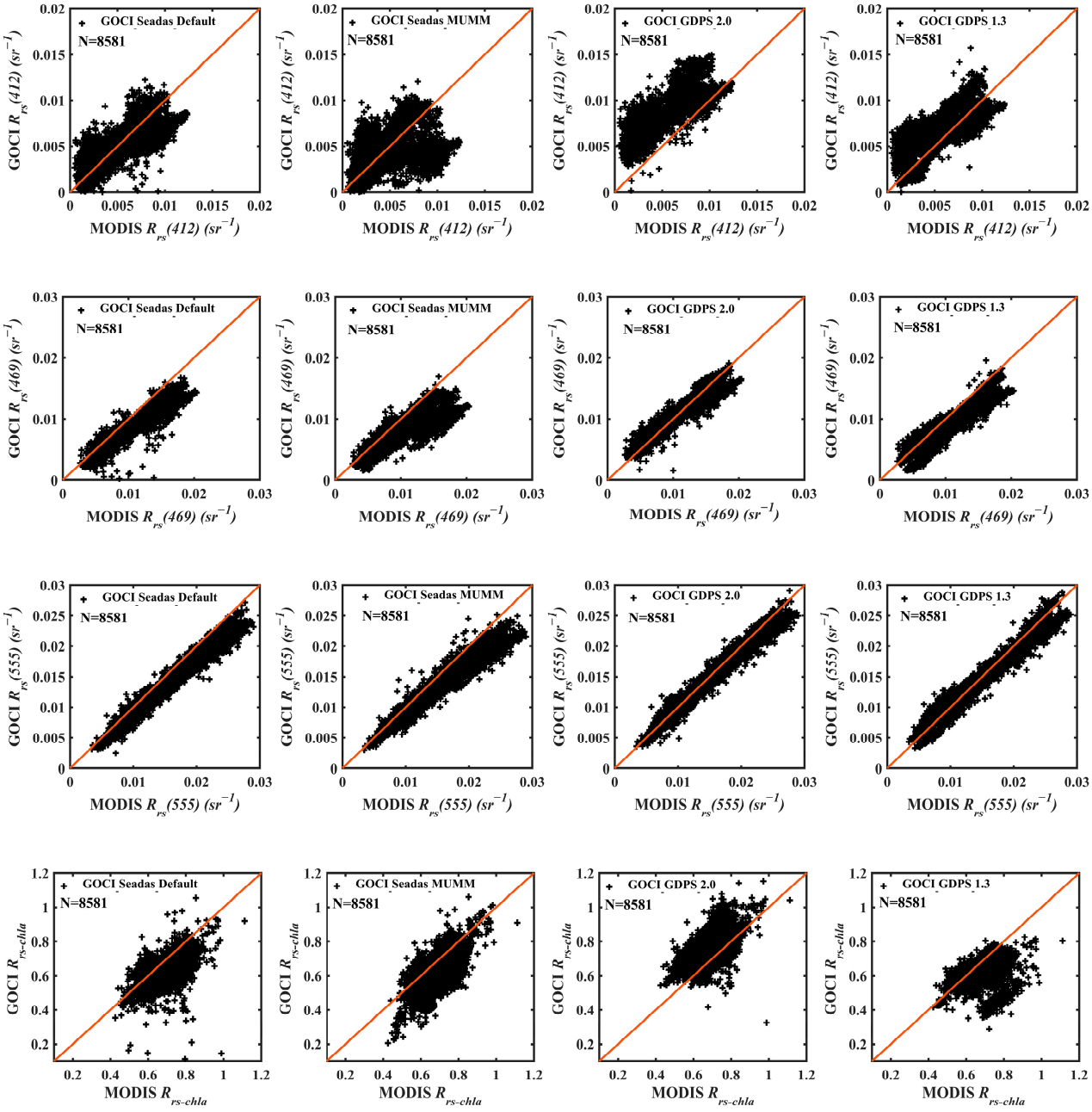

Figure 11. The scatter diagram of data comparison between GOCI and MODIS at 412 nm, 469 nm, 555 nm, and $R_{rs\text{-}chla}$ ($R_{rs\text{-}chla}$ = $R_{rs}(469)/R_{rs}(555)$). The abscissa represents MODIS R_{rs} data obtained from OBPG, and the ordinate represents GOCI R_{rs} data matching MODIS obtained from the four atmospheric-correction algorithms.

Table 6. The parameter values of the data-comparison scatter diagram between GOCI and MODIS at each band of the four atmospheric-correction algorithms.

Band (nm)	Atmospheric Correction Algorithms	r	ε	RMSE	QA Score
412	Seadas—Default	0.832	27.53%	0.00133	0.938
	Seadas—MUMM	0.580	38.72%	0.00199	0.922
	GDPS2.0	0.847	73.07%	0.00364	0.921
	GDPS1.3	0.800	56.70%	0.00247	0.967
443	Seadas—Default	0.932	15.96%	0.00129	0.938
	Seadas—MUMM	0.817	19.14%	0.00186	0.922
	GDPS2.0	0.939	26.39%	0.00181	0.921
	GDPS1.3	0.904	19.61%	0.00136	0.967
490	Seadas—Default	0.971	20.78%	0.00201	0.938
	Seadas—MUMM	0.939	19.70%	0.00230	0.922
	GDPS2.0	0.978	7.12%	0.00087	0.921
	GDPS1.3	0.962	9.38%	0.00126	0.967
531	Seadas—Default	0.985	16.24%	0.00197	0.938
	Seadas—MUMM	0.974	15.46%	0.00220	0.922
	GDPS2.0	0.986	5.29%	0.00091	0.921
	GDPS1.3	0.980	7.24%	0.00113	0.967
555	Seadas—Default	0.988	13.91%	0.00180	0.938
	Seadas—MUMM	0.979	13.32%	0.00204	0.922
	GDPS2.0	0.989	5.65%	0.00096	0.921
	GDPS1.3	0.982	7.68%	0.00112	0.967
660	Seadas—Default	0.982	30.57%	0.00129	0.938
	Seadas—MUMM	0.967	29.01%	0.00158	0.922
	GDPS2.0	0.983	10.04%	0.00063	0.921
	GDPS1.3	0.977	24.88%	0.00105	0.967

Table 7. The parameter values of the four GOCI atmospheric-correction algorithms in $R_{rs}(469)$, $R_{rs}(555)$, and $R_{rs\text{-}chla}$ compared with MODIS data. $R_{rs}(469)$ was generated by linear interpolation model from the existing GOCI bands. $R_{rs\text{-}chla} = R_{rs}(469)/R_{rs}(555)$.

R_{rs}	Atmospheric Correction Algorithms	ε	RMSE	QA Score
$R_{rs}(469)$	Seadas—Default	23.91%	0.00212	0.938
	Seadas—MUMM	22.62%	0.00248	0.922
	GDPS2.0	9.42%	0.00102	0.921
	GDPS1.3	11.98%	0.00153	0.967
$R_{rs}(555)$	Seadas—Default	13.91%	0.00180	0.938
	Seadas—MUMM	13.32%	0.00204	0.922
	GDPS2.0	5.65%	0.00096	0.921
	GDPS1.3	7.68%	0.00112	0.967
$R_{rs\text{-}chla}$	Seadas—Default	10.65%	0.08833	0.938
	Seadas—MUMM	10.79%	0.08751	0.922
	GDPS2.0	10.81%	0.09669	0.921
	GDPS1.3	9.70%	0.08674	0.967

Although the QA score is quite good for any atmospheric-correction algorithm, the difference of $R_{rs}(\lambda)$ between GOCI and MODIS may be large at a single band (Table 7). For example, the error at 469 nm is in a range of 9.42–23.91% for different atmospheric-correction algorithms, while the error at 555 nm is smaller than that at 469 nm, i.e., 5.65–13.91%. However, the error of the band ratio of $R_{rs}(469)/R_{rs}(555)$ is high in a range of 9.70–10.81%. The comparison of $R_{rs}(\lambda)$ between GOCI and MODIS also indicates that the QA score

system is helpful in measuring the spectral shape of $R_{rs}(\lambda)$ and evaluating the band ratio for developing bio-geochemical algorithms.

4. Discussion

It is traditional to validate ocean color measurements of $R_{rs}(\lambda)$ by comparing them with field measurements. In 2019, Huang et al. [37] used in situ measured R_{rs} to statistically analyze the suitability of four atmospheric-correction algorithms for GOCI data in the Yellow Sea. This is useful to evaluate the accuracy of retrieval of $R_{rs}(\lambda)$ at a single band. However, it does not evaluate the whole spectrum as a unified spectral curve. The QA score system overcomes the limitation of lack of in situ match-up data and measures the whole $R_{rs}(\lambda)$ spectrum. The research results of our study have indicated that even if the R_{rs} value of a single band is closer to the in situ measured value, there may be a big difference in the band ratio between the ocean color and the in situ measurements, which means a large difference in the $R_{rs}(\lambda)$ spectral shape. Therefore, it is of great significance to evaluate the quality of the whole spectrum using the QA score system in developing a bio-optical algorithm. Based on the analysis of this study (Sections 3.1 and 3.4), the Seadas—Default atmospheric-correction algorithm would be recommended to process GOCI L1B data if only the R_{rs} values at 412 nm and 443 nm are used in the Bohai Sea areas. The GDPS2.0 atmospheric-correction algorithm would be better when using the R_{rs} values at 490 nm, 531 nm, 555 nm, and 660 nm. However, if the band-ratio of $R_{rs}(\lambda)$ are applied for the development of bio-optical models in the Bohai Sea areas, the GDPS1.3 (or GDPS1.4*) atmospheric-correction algorithm can be considered.

In this study, MODIS L2 $R_{rs}(\lambda)$ data were used as the data set to evaluate the spectral quality of GOCI $R_{rs}(\lambda)$, rather than operational $R_{rs}(\lambda)$ products of other ocean color sensors. Firstly, in 2016, Shang et al. [49] clearly showed that in the Bohai Sea, MODIS L2 R_{rs} data provided by OBPG have good consistency with the measured in situ R_{rs} data (refer to Figures 2 and 3 of their paper) by comparing 20 sets of in situ measurements with the match-up MODIS satellite data. Secondly, the atmospheric-correction algorithm used by NASA OBPG to obtain MODIS L2 R_{rs} includes an optical model for turbidity and optically complex waters, which makes MODIS L2 R_{rs} data valid in this area [50]. In this study, there are only seven sets of GOCI and in situ match-up measurements in total. However, this is enough for illustrating that the QA score system is more helpful in evaluating the spectral data. A greater amount of field measurements is much better for further statistical analysis.

5. Conclusions

The remote sensing reflectance spectrum is of great importance in the retrieval of bio-geo-optical parameters of seawater from ocean color remote sensing. GOCI can provide eight observations of the $R_{rs}(\lambda)$ spectra every day. In practical work, atmospheric correction is the key factor to obtaining accurate spectral data of $R_{rs}(\lambda)$. In this study, the adaptability of four atmospheric-correction algorithms for deriving GOCI $R_{rs}(\lambda)$ measurements in the Bohai Sea were evaluated and analyzed based on the QA score spectral quality evaluation system. The results demonstrate that in any area of the Bohai Sea, the probability that the QA score of $R_{rs}(\lambda)$ equals 1 is higher when using the GDPS1.3 atmospheric-correction algorithm instead of the other three atmospheric-correction algorithms. Over 90% of the $R_{rs}(\lambda)$ data are of good quality with a score $\geq$4/6 for the GDPS1.3 algorithm. For any atmospheric-correction algorithm, the QA score is higher in the Three Bays (i.e., Bohai Bay, Liaodong Bay, and Laizhou Bay) than that in the central parts of the Bohai Sea.

The comparison of GOCI $R_{rs}(\lambda)$ with in situ and MODIS measurements of $R_{rs}(\lambda)$ indicates that the QA score system is valid in measuring $R_{rs}(\lambda)$ spectral shape. Therefore, the QA score has a higher correlation with the accuracy of R_{rs} band ratio rather than the accuracy of R_{rs} at a single band. For example, the in situ match-up data illustrate that the $R_{rs}(\lambda)$ from GDPS1.3 with a high QA score are not always in the best agreement with the in situ $R_{rs}(\lambda)$ at a single band. At the same time, the error of the $R_{rs}(\lambda)$ band ratio is the smallest. The actual meaning of scatter plots of GOCI vs. MODIS $R_{rs}(\lambda)$ data at a single band cannot

express the quality of the complete $R_{rs}(\lambda)$ spectrum clearly. It is necessary to evaluate and analyze the spectral quality overall. According to the result of this study, it is suggested that the GDPS1.3 (or GDPS1.4*) atmospheric-correction algorithm be used when using the band ratio of $R_{rs}(\lambda)$ for the development of bio-optical models in the Bohai Seas. The results of this study also provide a new idea for the selection of the atmospheric-correction algorithms. The hourly variation of QA score between UTC 00:16–07:16 demonstrates that the data quality of GOCI $R_{rs}(\lambda)$ can vary on an hour scale. When using GOCI measurements at eight observation times to study the variation of dynamical changes, the GOCI data with high quality should be selected with caution.

Author Contributions: Data Curation, X.L. and Y.Z.; Methodology, X.L.; Resources, Y.W.; Validation, X.L. and Q.Y.; Writing—Original Draft, X.L. and Q.Y.; Writing—Review and Editing, X.L., Q.Y. and Y.Z. All authors have read and agreed to the published version of the manuscript.

Funding: This research was funded by the National Key Research and Development Program of China, grant number 2019YFC1408003, and the Natural Science Foundation of Shandong Province, grant number ZR2019PD021.

Data Availability Statement: The data presented in this study are available on request from the corresponding author.

Acknowledgments: We express the gratitude of our team to the KOSC for providing us access to GOCI data and GDPS software. Additionally, we are also grateful to the NASA Ocean Biology Processing Group for providing us with the MODIS/Aqua data and SeaDAS software. Finally, we would like to thank Wei et al. for providing the source code of the QA score.

Conflicts of Interest: The authors declare no conflict of interest.

References

1. Lee, Z.; Carder, K.L.; Arnone, R.A. Deriving inherent optical properties from water color: A multi-band quasi-analytical algorithm for optically deep waters. *Appl. Opt.* **2002**, *41*, 5755–5772. [CrossRef] [PubMed]
2. Morel, A.; Prieur, L. Analysis of variations in ocean color. *Limnol. Oceanogr.* **1977**, *22*, 709–722. [CrossRef]
3. Ryu, J.-H.; Han, H.-J.; Cho, S.; Park, Y.-J.; Ahn, Y.-H. Overview of geostationary ocean color imager (GOCI) and GOCI data processing system (GDPS). *Ocean Sci. J.* **2012**, *47*, 223–233. [CrossRef]
4. Kim, D.-W.; Park, Y.-J.; Jeong, J.-Y.; Jo, Y.-H. Estimation of Hourly Sea Surface Salinity in the East China Sea Using Geostationary Ocean Color Imager Measurements. *Remote Sens.* **2020**, *12*, 755. [CrossRef]
5. Cao, H.; Han, L. Hourly remote sensing monitoring of harmful algal blooms (HABs) in Taihu Lake based on GOCI images. *Environ. Sci. Pollut. Res.* **2021**, *28*, 35958–35970. [CrossRef]
6. Kim, W.; Moon, J.-E.; Park, Y.-J.; Ishizaka, J. Evalution of chlorophyll retrievals from Geostationary Ocean color Imager (GOCI) for the North-East Asian region. *Remote Sens. Environ.* **2016**, *184*, 482–495. [CrossRef]
7. Ling, Z.; Sun, D.; Wang, S.; Qiu, Z.; Huan, Y.; Mao, Z.; He, Y. Remote sensing estimation of colored dissolved organic matter (CDOM) from GOCI measurements in the Bohai Sea and Yellow Sea. *Environ. Sci. Pollut. Res.* **2020**, *27*, 6872–6885. [CrossRef]
8. Bai, S.; Gao, J.; Sun, D.; Tian, M. Monitoring Water Transparency in Shallow and Eutrophic Lake Waters Based on GOCI Observations. *Remote Sens.* **2020**, *12*, 163. [CrossRef]
9. Hsu, P.-C.; Lu, C.-Y.; Hsu, T.-W.; Ho, C.-R. Diurnal to Seasonal Variations in Ocean Chlorophyll and Ocean Currents in the North of Taiwan Observed by Geostationary Ocean Color Imager and Coastal Radar. *Remote Sens.* **2020**, *12*, 2853. [CrossRef]
10. Minghelli, A.; Lei, M.; Charmasson, S.; Rey, V.; Chami, M. Monitoring Suspended Particle Matter Using GOCI Satellite Data after the Tohoku (Japan) Tsunami in 2011. *IEEE J. Sel. Top. Appl. Earth Obs. Remote Sens.* **2019**, *12*, 567–576. [CrossRef]
11. Mao, Y.; Wang, S.; Qiu, Z.; Sun, D.; Bilal, M. Variations of transparency derived from GOCI in the Bohai Sea and the Yellow Sea. *Opt. Express* **2018**, *26*, 12191–12209. [CrossRef] [PubMed]
12. Gordon, H.R. Removal of atmospheric effects from satellite imagery of the oceans. *Appl. Opt.* **1978**, *17*, 1631–1636. [CrossRef] [PubMed]
13. Gordon, H.R.; Wang, M. Retrieval of water leaving radiance and aerosol optical thickness over the oceans with SeaWiFS: A preliminary algorithm. *Appl. Opt.* **1994**, *33*, 443–452. [CrossRef] [PubMed]
14. Siegel, D.A.; Wang, M.; Maritorena, S.; Robinson, W. Atmospheric correction of satellite ocean color imagery: The black pixel assumption. *Appl. Opt.* **2000**, *39*, 3582–3591. [CrossRef]
15. Wang, M.; Knobelspiesse, K.D.; McClain, C.R. Study of the Sea-Viewing Wide Field-of-View Sensor (SeaWiFS) aerosol optical property data over ocean in combination with the ocean color products. *J. Geophys. Res.* **2005**, *110*, 1–14. [CrossRef]
16. Jamet, C.; Loisel, H.; Kuchinke, C.P. Comparison of three SeaWiFS atmospheric correction algorithms for turbid waters using AERONET-OC measurements. *Remote Sens. Environ.* **2011**, *115*, 1955–1965. [CrossRef]

17. Goyens, C.; Jamet, C.; Schroeder, T. Evaluation of four atmospheric correction algorithms for MODIS-Aqua images over contrasted coastal waters. *Remote Sens. Environ.* **2013**, *131*, 63–75. [CrossRef]
18. Ahn, J.-H.; Park, Y.-J. Estimating Water Reflectance at Near-Infrared Wavelengths for Turbid Water Atmospheric Correction: A Preliminary Study for GOCI-II. *Remote Sens.* **2020**, *12*, 3791. [CrossRef]
19. Wang, M.; Shi, W. The NIR-SWIR combined atmospheric correction approach for MODIS ocean color data processing. *Opt. Express* **2007**, *15*, 15722–15733. [CrossRef]
20. Wang, M.; Shi, W. Remote Sensing of the Ocean Contributions from Ultraviolet to Near-Infrared Using the ShortwaveInfrared Bands: Simulations. *Appl. Opt.* **2007**, *46*, 1535–1547. [CrossRef]
21. Oo, M.; Vargas, M.; Gilerson, A.; Gross, B.; Moshary, F.; Ahmed, S. Improving atmospheric correction for highly productive coastal waters using the short wave infrared retrieval algorithm with water-leaving reflectance constraints at 412 nm. *Appl. Opt.* **2008**, *47*, 3846–3859. [CrossRef] [PubMed]
22. He, X.; Bai, Y.; Pan, D.; Junwu, T.; Difeng, W. Atmospheric correction of satellite ocean color imagery using the ultraviolet wavelength for highly turbid waters. *Opt. Express* **2012**, *20*, 20754–20770. [CrossRef] [PubMed]
23. Hu, C.; Carder, K.L.; Muller-Karger, F.E. Atmospheric correction of SeaWiFS imagery over turbid coastal waters: A practical method. *Remote Sens. Environ.* **2000**, *74*, 195–206. [CrossRef]
24. Ruddick, K.G.; Ovidio, F.; Rijkeboer, M. Atmospheric correction of SeaWiFS imagery for turbid coastal and inland waters. *Appl. Opt.* **2000**, *39*, 897–912. [CrossRef]
25. Wang, M.; Shi, W.; Jiang, L. Atmospheric correction using near-infrared bands for satellite ocean color data processing in the turbid western Pacific region. *Opt. Express* **2012**, *20*, 741–753. [CrossRef]
26. Ahn, J.-H.; Park, Y.-J.; Fukushima, H. Comparison of Aerosol Reflectance Correction Schemes Using Two Near-Infrared Wavelengths for Ocean Color Data Processing. *Remote Sens.* **2018**, *10*, 1791. [CrossRef]
27. AHN, J.-H.; PARK, Y.-J.; KIM, W.; LEE, B. Simple aerosol correction technique based on the spectral relationships of the aerosol multiple-scattering reflectances for atmospheric correction over the oceans. *Opt. Express* **2016**, *24*, 29659–29669. [CrossRef]
28. Stumpf, R.P.; Arnone, R.A.; Gould, R.W.; Martinolich, P.M.; Ransibrahmanakul, V. A Partially Coupled Ocean-Atmosphere Model for Retrieval of Water-Leaving Radiance from SeaWiFS in Coastal Waters. *NASA Tech. Memo.* **2003**, *206892*, 51–59.
29. Lavender, S.J.; Pinkerton, M.H.; Moore, G.F.; Aiken, J.; Blondeau-Patissier, D. Modification to the atmospheric correction of SeaWiFS ocean colour images over turbid waters. *Cont. Shelf Res.* **2005**, *25*, 539–555. [CrossRef]
30. Jamet, C.; Thiria, S.; Moulin, C. Use of a Neurovariational Inversion for Retrieving Oceanic and Atmospheric Constituents from Ocean Color Imagery: A Feasibility Study. *J. Atmos. Ocean. Tech.* **2005**, *22*, 460–475. [CrossRef]
31. Schroeder, T.; Behnert, I.; Schaale, M.; Fischer, J.; Doerffer, R. Atmospheric correction algorithm for MERIS above case-2 waters. *J. Remote Sens.* **2007**, *28*, 1469–1486. [CrossRef]
32. Brajard, J.; Santer, R.; Crpon, M.; Thiria, S. Atmospheric correction of MERIS data for case-2 waters using a neuro-variational inversion. *Remote Sens. Environ.* **2012**, *126*, 51–61. [CrossRef]
33. Brajard, J.; Jamet, C.; Thiria, S.; Moulin, C.; Crepon, M. Use of a neuro-variational inversion for retrieving oceanic and atmospheric constituents from satellite ocean color sensor: Application to absorbing aerosols. *Neural Netw.* **2006**, *22*, 460–475. [CrossRef]
34. Kuchinke, C.P.; Gordon, H.R.; Harding, L.W.; Voss, K.J. Spectral optimization for constituent retrieval in Case II waters II: Validation study in the Chesapeake Bay. *Remote Sens. Environ.* **2009**, *113*, 610–621. [CrossRef]
35. Chomko, R.; Gordon, H.; Maritorena, S.; Siegel, D. Simultaneous retrieval of oceanic and atmospheric parameters for ocean color imagery by spectral optimization: A validation. *Remote Sens. Environ.* **2003**, *84*, 208–220. [CrossRef]
36. Zibordi, G.; Berthon, J.-F.; Melin, F.; Alimonte, D.; Kaitala, S. Validation of satellite ocean color primary products at optically complex coastal sites: Northern Adriatic Sea, Northern Baltic Proper and Gulf of Finland. *Remote Sens. Environ.* **2009**, *113*, 2574–2591. [CrossRef]
37. Huang, X.; Zhu, J.; Han, B.; Jamet, C.; Tian, Z.; Zhao, Y.; Li, J.; Li, T. Evaluation of Four Atmospheric Correction Algorithms for GOCI Images over the Yellow Sea. *Remote Sens.* **2019**, *11*, 1631. [CrossRef]
38. Zhang, M.; Hu, C.; Cannizzaro, J.; English, D.; Barnes, B.B.; Carlson, P.; Yarbro, L. Comparison of two atmospheric correction approaches applied to MODIS measurements over North American waters. *Remote Sens. Environ.* **2018**, *216*, 442–455. [CrossRef]
39. Bailey, S.W.; Werdell, P.J. A multi-sensor approach for the on-orbit validation of ocean color satellite data products. *Remote Sens. Environ.* **2006**, *102*, 12–23. [CrossRef]
40. Salama, M.S.; Stein, A. Error decomposition and estimation of inherent optical properties. *Appl. Opt.* **2009**, *48*, 4947–4962. [CrossRef] [PubMed]
41. Wang, M.; Son, S. VIIRS-derived chlorophyll-a using the ocean color index method. *Remote Sens. Environ.* **2016**, *182*, 141–149. [CrossRef]
42. Guo, S.; Sun, B.; Zhang, H.K.; Liu, J.; Chen, J.; Wang, J.; Jiang, X.; Yang, Y. MODIS ocean color product downscaling via spatio-temporal fusion and regression: The case of chlorophyll-a in coastal waters. *Int. J. Appl. Earth Obs. Geoinf.* **2018**, *73*, 340–361. [CrossRef]
43. Wei, J.; Lee, Z.; Shang, S. A system to measure the data quality of spectral remote sensing reflectance of aquatic environments. *J. Geophys. Res. Ocean.* **2016**, *121*, 8189–8207. [CrossRef]
44. Ahn, J.H.; Park, Y.J.; Kim, W.; Lee, B. Vicarious calibration of the geostationary ocean color imager. *Opt. Express* **2015**, *23*, 23236–23258. [CrossRef]

45. Ahn, J.-H.; Park, Y.-J.; Ryu, J.-H.; Lee, B.; Oh, I.S. Development of atmospheric correction algorithm for Geostationary Ocean Color Imager (GOCI). *Ocean. Sci. J.* **2012**, *47*, 247–259. [CrossRef]
46. He, M.; He, S.; Zhang, X.; Zhou, F.; Li, P. Assessment of Normalized Water-Leaving Radiance Derived from GOCI Using AERONET-OC Data. *Remote Sens.* **2021**, *13*, 1640. [CrossRef]
47. Chavula, G.; Brezonik, P.; Thenkabail, P.; Johnson, T.; Bauer, M. Estimating chlorophyll concentration in Lake Malawi from MODIS satellite imagery. *Phys. Chem. Earth Parts A/B/C* **2009**, *34*, 755–760. [CrossRef]
48. NASA SeaDAS. Available online: https://seadas.gsfc.nasa.gov/history/ (accessed on 15 June 2021).
49. Shang, S.; Lee, Z.; Shi, L.; Lin, G.; Wei, G.; Li, X. Changes in water clarity of the Bohai Sea: Observations from MODIS. *Remote Sens. Environ.* **2016**, *186*, 22–31. [CrossRef]
50. Bailey, S.W.; Franz, B.A.; Werdell, P.J. Estimation of near-infraredwater-leaving reflectance for satellite ocean color data processing. *Opt. Express* **2010**, *18*, 7521–7527. [CrossRef]
51. Kruse, F.A.; Lefkoff, A.B.; Boardman, J.B.; Heidebrecht, K.B.; Shapiro, A.T.; Barloon, P.J.; Goetz, A.F.H. The spectral image processing system (SIPS)—Interactive visualization and analysis of imaging spectrometer data. *Remote Sens. Environ.* **1993**, *44*, 145–163. [CrossRef]